THE ASTROPHYSICAL JOURNAL, 473:1079–1088, 1996 December 20

PULSATIONS AND LINE PROFILE CHANGES IN THE ULTRAVIOLET SPECTRUM OF HERCULES X-1: RESULTS FROM A MULTIWAVELENGTH CAMPAIGN

BRAM BOROSON AND S. D. VRTILEK
Center for Astrophysics, 60 Garden Street, Cambridge, MA 02138; bboroson@head-cfa.harvard.edu, saku@head-cfa.harvard.edu
RICHARD MCCRAY
Joint Institute for Laboratory Astrophysics, Campus Box 440, University of Colorado, Boulder, CO 80309; dick@jila.colorado.edu
TIMOTHY KALLMAN
Goddard Spaceflight Center, Greenbelt, MD 20771; tim@xstar.gsfc.nasa.gov
AND
FUMIAKI NAGASE
Institute for Space and Astronautical Science, 3-1-1, Yoshinodai, Sagamihara, Kanagawa 229, Japan
Received 1996 March 26; accepted 1996 July 15

ABSTRACT

We report simultaneous X-ray and ultraviolet observations of the X-ray binary pulsar Hercules X-1, obtained over nearly half of a 1.7 day binary orbit using the *ASCA* X-ray telescope and the Goddard High Resolution Spectrograph (GHRS) aboard the *Hubble Space Telescope*. The GHRS resolved, for the first time, two moving emission components. One feature in the N v $\lambda\lambda$1238.8, 1242.8 doublet is broad (FWHM $\approx$ 1000 km s^{-1}) and the other is narrow (FWHM $\approx$ 150 km s^{-1}). We attribute the broad emission line to the X-ray–illuminated surface of a Keplerian accretion disk and the narrow line to the X-ray–heated atmosphere of the companion star, HZ Her. Near orbital phase $\phi_{\rm orb} = 0.80$ (simultaneous with a pre-eclipse X-ray dip), the N v λ1242.8 component became stronger than the N v λ1238.8 component. Later in the orbit, the blue edge of the broad lines diminished as the approaching side of the accretion disk was occulted by HZ Her. UV continuum pulsations were detected for the first time, with an amplitude $\approx$0.5% of the steady flux. The pulse shapes of the UV continuum and hard X-rays were similar at $\phi_{\rm orb} = 0.83$ but not at $\phi_{\rm orb} = 0.56$. We found evidence for a stronger pulsation (amplitude $\approx$15%) within a narrow (0.25 Å) segment of the broad 1242.8 Å N v component, only at $\phi_{\rm orb} = 0.80$. We briefly discuss some implications of these observations for the gas flows in the Her X-1 system.

Subject headings: binaries: eclipsing — stars: individual (Hercules X-1) — ultraviolet: stars — X-rays: stars

1. INTRODUCTION

Hercules X-1 (discovered by Tananbaum et al. 1972) is at once one of the most well-studied and enigmatic of the X-ray binaries. It pulses in X-rays every 1.24 s as a spinning, accreting neutron star brings its magnetic poles alternately into and out of our line of sight. The X-rays are eclipsed every 1.7 days, a period also observed in modulations of the optical flux (Bahcall & Bahcall 1972; Milgrom & Salpeter 1975). This period is caused by the binary orbit of the neutron star with a $\sim 2\ M_\odot$ companion, HZ Her. There is still no satisfactory explanation for a 35 day cycle in which a "main-on" state (X-ray luminosity $L_{\rm X} \sim 10^{37}$ ergs s^{-1} for $\approx$8 days) and "short-on" state ($L_{\rm X}$ lower than in the main-on state by a factor $\sim$3 for $\approx$5 days) are separated by an "off-state" during which a residual X-ray luminosity of several percent of the main-on luminosity probably results from scattering by an accretion disk corona. Attempts to explain the 35 day period invoke a twisted, precessing accretion disk (Petterson 1975) which periodically blocks our line of sight. The cause of this precession, however, remains under dispute. X-ray dips (Giacconi et al. 1973) are observed near orbital phases $\phi_{\rm orb} = 0.55$ ("anomalous dips") and $\phi_{\rm orb} = 0.8$ ("pre-eclipse dips"), where $\phi_{\rm orb} = 0.0$ corresponds to mid-eclipse. The X-ray dips recur at a period of 1.62 days and may be caused by episodes of mass transfer at the beat period between the 1.7 day and 35 day periods (Crosa & Boynton 1980).

Previous observations with the *International Ultraviolet Explorer* (*IUE*; Dupree et al. 1978; Howarth & Wilson 1983; Boyle et al. 1986) revealed that the strongest emission lines in the optical/UV spectrum of Her X-1 are N v $\lambda\lambda$1238.8, 1242.8. The strength of the N v doublet and the weaker C IV $\lambda\lambda$1548,1550 vary over the orbit. Near X-ray eclipse, the flux in these doublets is greater than that predicted by models of the X-ray–heated surface of HZ Her. This suggests that most of the line flux near eclipse may originate in the accretion disk (Boyle et al. 1986).

IUE observations of the N v lines at high resolution (Howarth & Wilson 1983; Boyle et al. 1986) suggested that they are narrow (FWHM $\approx$ 100 km s^{-1}) and that they are caused either by discrete blobs orbiting the neutron star (Howarth & Wilson 1983) or by the X-ray–heated atmosphere of the normal star (Boyle et al. 1986). Observations of Her X-1 with the Faint Object Spectrograph (FOS) onboard the *Hubble Space Telescope* (Anderson et al. 1994; Cheng et al. 1995) showed the persistence of the UV lines (reduced by a factor of $\approx 10^2$) through the middle of the X-ray eclipse. However, the FOS was used with the large 4.″3 slit and before COSTAR was installed. As a result, the FOS observations were limited to a velocity resolution of $\approx$400 km s^{-1}.

The optical continuum of Her X-1 pulses at the neutron star period (Davidsen et al. 1975; Groth 1974), with rms amplitude $\sim 10^{-3}$ of the total optical intensity. From pulse

timing, two separate sources of these pulses have been distinguished (Middleditch & Nelson 1976). One source moves with HZ Her and appears strongest at $\phi_{orb} = 0.25$ and $\phi_{orb} = 0.75$. The other source moves with the neutron star and appears only at $\phi_{orb} \sim 0.8$.

Optical emission lines may also pulse, with amplitude greater than the continuum amplitude. Amplitudes of 2.5% (Davidsen et al. 1975) and 25% (Margon et al. 1976) have been reported for the He II, N III emission blend at $\lambda \sim 4650$ Å.

Clearly, Her X-1 is a complex system. Separate components emit, scatter, reprocess, and obscure the X-rays at a variety of periods, some of which remain unexplained. High-resolution spectroscopy of Doppler-shifted emission lines, a mainstay diagnostic of astrophysical flows, has not been used to full effect in the study of X-ray binaries. Current X-ray instruments lack the needed resolution, and the strongest optical/UV emission lines lie in the far-ultraviolet, where they are obscured by Earth's atmosphere and Galactic absorption. The Goddard High Resolution Spectrograph (GHRS; Soderblom et al. 1993) onboard the *Hubble Space Telescope* (*HST*) offered the opportunity to study the far-ultraviolet at the needed spectral resolution. Her X-1 was an ideal target for this study because its reddening is low, consistent with its distance of ≈ 3 kpc above the Galactic plane. The gas flows suggested by the variety of periodicities should be detectable as emission components with various Doppler velocities.

The GHRS observations reported here achieve velocity resolutions of 150 km s^{-1} (low resolution) and 15 km s^{-1} (medium resolution). This fulfills the first goal of our observation: to resolve the Keplerian rotation at the edge of the accretion disk (velocities ~ 300 km s^{-1}), the Doppler shifts due to the binary orbit ($\lesssim 150$ km s^{-1}), and the shapes of the narrow N V lines ($\lesssim 100$ km s^{-1}). Our second goal was to detect pulsations in the strong UV lines of Her X-1 and to correlate them with X-ray pulsations observed using *ASCA*. In combining high spectral resolution with high time resolution (power-spectral resolution), we have a powerful means to infer the kinematics of the accretion flows.

In this paper (Paper I), we present the results obtained with the GHRS, including the simultaneous detection of pulsations with the GHRS and *ASCA*. In Paper II, we will examine the shape and time-variability of the X-ray spectrum as observed with *ASCA*. Finally, in Paper III, we will interpret these observations with theoretical models of an accretion disk wind, the material that causes the pre-eclipse dips, and radiatively driven ablation from the surface of HZ Her.

2. OBSERVATION PLAN

The GHRS observations took place on 1994 August 27 (see Table 1), after the *HST* refurbishment mission that installed COSTAR. We alternated between the low-resolution (150 km s^{-1}) G140L grating and the medium-resolution (15 km s^{-1}) G140M grating. For both gratings, we used the Large Science Aperture, which has a field of view of 1.″74. For the medium-resolution observations, we observed the 35 Å region surrounding the N V doublet at 1238.8, 1242.8 Å.

The RAPID mode of the GHRS allows readouts as short as 50 ms, although the onboard tape recorder can only store data for about 20 minutes if the readout time is less than 0.35 s. For all but our first *HST* orbit, we employed a readout time of 0.35 s, sufficient to detect pulsations at the neutron star spin period (1.24 s). The 0.35 s readout allowed us to record data during the full ≈ 50 minute interval available during each orbit of the *HST*. During the first *HST* orbit, the spacecraft passed through the South Atlantic Anomaly, and, as a result, a shorter time was available for observing Her X-1. The limitation of a 20 minute exposure was therefore not severe during the first *HST* orbit, and during this interval we employed a readout time of 0.1 s.

Our observation began during the second 1.7 day orbit after X-ray turn-on (as observed with BATSE; R. Wilson & M. Finger 1994, private communication), or about 3.5 days after the nominal turn-on period (Ögelman 1987). Her X-1 had emerged from the anomalous low state observed during a previous multiwavelength campaign using *ASCA* (Vrtilek & Cheng 1996). Thus, the source was in a favorable state for simultaneous observations with *ASCA*.

Figure 1 shows the timing of the low- and medium-resolution GHRS observations in relation to the X-ray light curve we observed with *ASCA*. The *ASCA* light curve shows a pre-eclipse X-ray dip at $\phi = 0.8$, preceded by a period of intermittent obscuration at $\phi = 0.75$. A weaker anomalous dip was observed at $\phi = 0.53$.

TABLE 1

GHRS OBSERVATION PLAN FOR HER X-1

Observation	Low/Medium	Start Time (UT)	Length (s)	Phase	λ (Å)	Comments
2	L	3:13	1266	0.559	1200–1450	0.1 s readout, N V lines at max., continuum pulsed 0.3 % prominent O IV] 1400
4	L	4:46	729	0.596	1400–1650	C IV lines at maximum, prominent N IV] 1486
6	M	6:25	2311	0.641	1225–1255	Unusual trough blueward of red component of N V
8	M	7:59	2474	0.680	1225–1255	
A	L	9:36	911	0.715	1200–1450	N V lines broaden, Si IV is double-peaked
C	L	9:55	963	0.723	1400–1650	C IV doublet merges, Si IV is double-peaked
E	M	11:13	2431	0.760	1225–1255	Broad N V moves to the red, narrow N V moves to the blue
G	M	12:49	2475	0.799	1225–1255	Broad N V lines show reversed doublet ratio and are at maximum. Pulsations in red component, 15% rms pulsed fraction
I	L	14:26	911	0.833	1200–1450	Pulsed continuum, lines double-peaked
K	L	14:44	969	0.841	1400–1650	Lines double-peaked
M	M	16:03	2413	0.878	1225–1255	Narrow lines have disappeared
O	M	17:38	1585	0.914	1225–1255	Blue part of broad line decreases

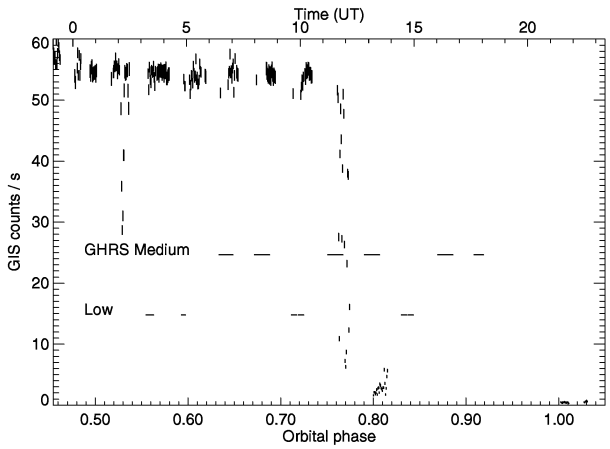

FIG. 1.—*ASCA* light curve of Her X-1. Times of the simultaneous GHRS exposures are indicated by the horizontal lines. Horizontal lines labeled "medium" correspond to the GHRS exposures using the G140M grating, with ≈ 15 km s^{-1} resolution, while lines labeled "low" correspond to the G140L grating, with ≈ 150 km s^{-1} resolution. The *ASCA* light curve shows an anomalous dip at $\phi_{orb} = 0.53$, a pre-eclipse dip at $\phi_{orb} = 0.8$, and X-ray eclipse centered at $\phi_{orb} = 0.0$. The *ASCA* light curve includes counts from the GIS 2 and GIS 3 in both medium and high bit rate. The count rates observed with medium bit rate have been scaled to agree with the counts observed at high bit rate.

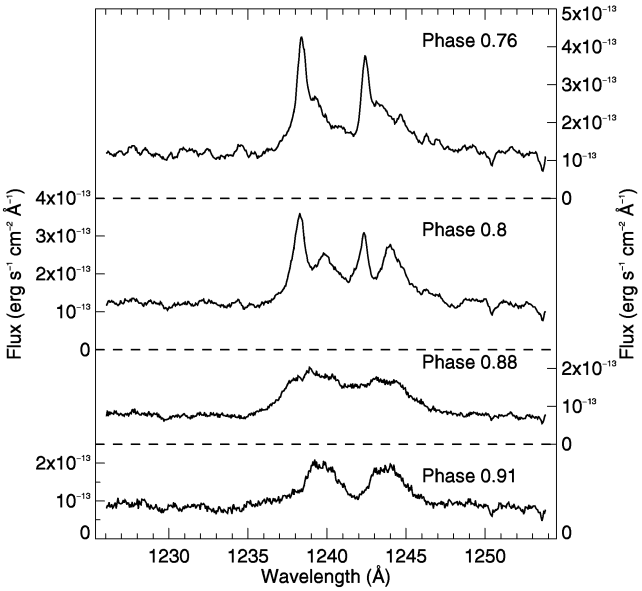

FIG. 2.—Medium-resolution spectra of the N v lines of Her X-1 obtained with the GHRS at four orbital phases. The spectra have been smoothed with a Weiner filter.

An *HST* guide star calibration immediately preceding our observation accidentally left the spacecraft in a mode in which we were unable to fix onto guide stars or to use the "fine-lock" mode (which allows an rms jitter of only 0.″005). However, the agreement between the UV fluxes we observed and those observed previously suggests that Her X-1 was nearly centered in the spectroscopic slit. The "coarse-lock" mode should only introduce a jitter of 0.″015 (insignificant if HZ Her/Her X-1 is nearly centered in the 1.″74 slit) and at periods uncorrelated with the neutron star rotation period.

3. MEDIUM-RESOLUTION OBSERVATIONS OF THE N v DOUBLET

Our medium-resolution observations have found, for the first time, two spectroscopically distinct emission sources in Her X-1. One component is a narrow (≈ 150 km s^{-1} FWHM) feature, which steadily decreases in brightness from $\phi_{orb} = 0.55$ to $\phi_{orb} = 0.88$, when it becomes invisible. Figure 2 shows the progression of medium-resolution spectra from $\phi_{orb} = 0.76$ to $\phi_{orb} = 0.91$. The broad component is overwhelmed by the greater flux of the narrow component at early orbital phases, starts to become brighter at $\phi_{orb} = 0.76$, and is seen most clearly after $\phi_{orb} = 0.88$ (when the narrow component is not seen). The medium-resolution observations are summarized in Table 2. Velocities have been calibrated with the "SPYBAL" spectral lamp calibration exposures taken before each *HST* orbit.

Both the narrow and broad components shift wavelengths as the orbit progresses. The narrow component moves toward the blue, while the broad component initially moves to the red (from underneath a stronger narrow component which masks its presence before $\phi_{orb} = 0.76$) and then moves to the blue. When we compare (Fig. 3) the Doppler velocity of the broad and narrow components with the Doppler velocities expected from the neutron star, the center of mass of HZ Her, and the L1 Lagrangian point, we conclude that the broad lines are probably associated with the neutron star and the narrow lines with HZ Her.

We have assumed the Her X-1 system has a recession velocity of 40 km s^{-1}, consistent with the interstellar S II absorption lines at 1250.578, 1253.805 Å (Table 2). Crampton & Hutchings (1974) inferred a systemic velocity

TABLE 2

VELOCITIES, FLUXES, AND EQUIVALENT WIDTHS OF LINES IN MEDIUM-RESOLUTION EXPOSURES

Line	λ_{lab} (Å)	ϕ_{orb}	Flux[a]	EW[b]	Velocity[c]
N v.....	1238.821	0.641	3.06(−13)	−1.511	−25
N v.....	1238.821	0.680	2.57(−13)	−1.300	−75
N v.....	1238.821	0.760	1.27(−13)	−0.533	−107
N v.....	1238.821	0.799	1.25(−13)	−0.757	+249
N v.....	1238.821	0.799	1.74(−13)	−1.030	−114
N v.....	1238.821	0.878	2.7(−13)	−2.5	+96
N v.....	1238.821	0.914	1.7(−13)	−1.5	+211
N v.....	1242.804	0.641	2.46(−13)	−1.299	−17
N v.....	1242.804	0.680	1.89(−13)	−0.966	−75
N v.....	1242.804	0.760	9.53(−14)	−0.473	−102
N v.....	1242.804	0.799	1.02(−13)	−0.599	−113
N v.....	1242.804	0.799	1.51(−13)	−0.937	+290
N v.....	1242.804	0.878	1.9(−13)	−1.8	+96
N v.....	1242.804	0.914	1.6(−13)	−1.5	+221
S II	1250.578	0.641	abs	0.096	−41
S II	1250.578	0.680	abs	0.185	−35
S II	1250.578	0.760	abs	0.099	−37
S II	1250.578	0.799	abs	0.084	−34
S II	1250.578	0.878	abs	0.081	−39
S II	1250.578	0.914	abs	0.083	−36
S II	1253.805	0.641	abs	>0.095	−41
S II	1253.805	0.680	abs	> 0.095	−43
S II	1253.805	0.760	abs	> 0.098	−39
S II	1253.805	0.799	abs	0.097	−42
S II	1253.805	0.878	abs	0.110	−36
S II	1253.805	0.914	abs	0.100	−48

[a] In ergs s^{-1} cm^{-2} Å^{-1}; "abs" indicates an absorption line.
[b] Equivalent width in Å.
[c] In km s^{-1} of peak. For the broad redshifted lines at $\phi_{orb} = 0.878$, 0.914, we use the average of the half-maximum velocities.

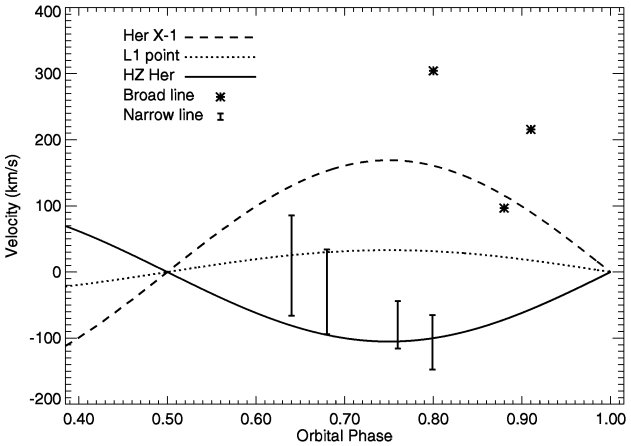

FIG. 3.—Doppler velocities expected for the motion of the neutron star, the L1 Lagrangian point, and the center of mass of HZ Her are compared with the velocities observed in the narrow and broad lines. The error bars represent the velocities of the half-maxima of the narrow lines, averaged over the two doublet components. The asterisks represent the average of the velocities of the half-maxima of the broad lines. The velocities are relative to the S II lines, which we assume are interstellar.

of 60 km s^{-1} from models of absorption line variations. This is not far from the velocity of the S II lines and does not change our identification of the broad and narrow components with the disk and normal star.

We determined the broad line velocities for Figure 3 by averaging the velocities at either side of the broad peak where the flux reaches half the maximum value. When the doublet components did not overlap, we averaged the velocities determined from each separate component. At $\phi = 0.88$, where the doublet components overlap, we used the blue edge of the 1238.8 Å line and the red edge of the 1242.8 Å line to measure the half-maximum velocities. While Figure 3 shows that the broad lines move with Doppler velocities closer to those expected from the neutron star than from HZ Her, there are also large deviations at $\phi = 0.80$ and $\phi = 0.91$. In Paper II we propose that at $\phi = 0.80$ the broad lines have a P Cygni profile and that at $\phi_{orb} = 0.91$ the accretion disk is partially occulted by HZ Her (see also § 3.1).

At $\phi_{orb} = 0.64$, the Doppler velocity of the narrow N v lines are near the velocity expected from the L1 Lagrangian point. Later in the orbit, the N v line velocities are near the Doppler velocity of the center of mass of HZ Her (Fig. 3). The doublet ratio (F_{1238}/F_{1242}) in the narrow N v lines is $\approx$1.2–1.4, indicating that the emitting gas has optical depth $\tau \sim 1$.

3.1. *Broad Emission Component: Reversal of the* N v *Doublet ratio*

Our observation at $\phi_{orb} = 0.80$ (Fig. 2) shows that in the peak of the broad emission line at (heliocentric) velocity

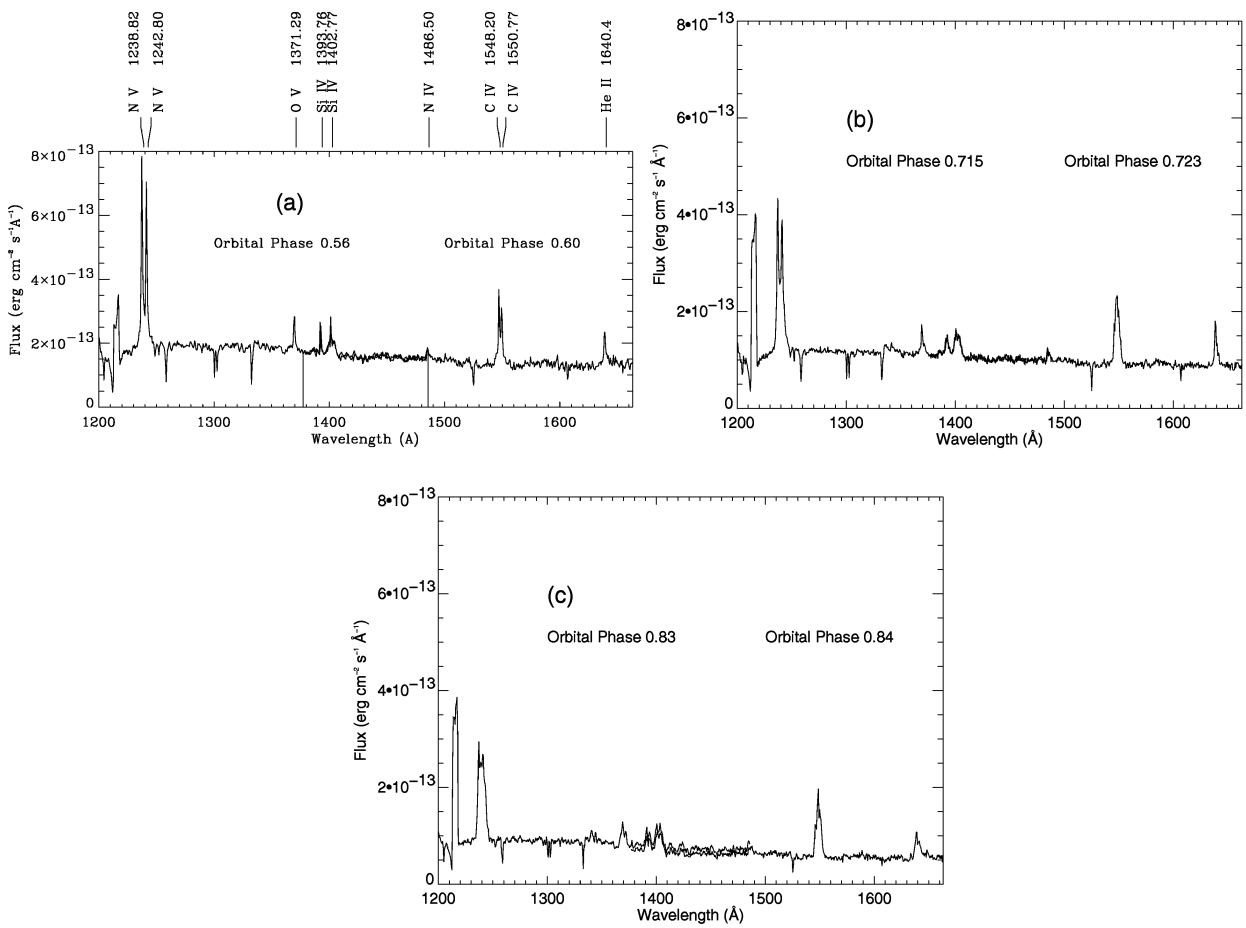

FIG. 4.—Low-resolution observations of the UV spectrum of Her X-1. We combine spectra taken at closely spaced orbital phases to increase our wavelength range. (*a*) Observations at $\phi_{orb} = 0.56$, 0.6. The vertical breaks in the spectra indicate the wavelength extent of the exposures, which overlap from 1380 Å to 1490 Å. Prominent emission lines are labeled. (*b*) Observations at $\phi_{orb} = 0.71$, 0.72. (*c*) Observations at $\phi_{orb} = 0.83$, 0.84.

TABLE 3

EMISSION AND ABSORPTION LINES FROM HER X-1 DETECTED WITH THE LOW-RESOLUTION G140L GRATING

Ion	λ_{lab} (Å)	ϕ_{orb}	Total Flux[a]	Velocity[b]
N v	1238,1242	0.559	1.89(−12)	−309,−298
N v	1238,1242	0.715	1.52(−12)	−306,−296
N v	1238,1242	0.833	1.35(−12)	−286,−306
S II	1250.578	0.559	abs	−401
S II	1250.578	0.715	abs	−362
S II	1253.805	0.559	abs	−335
S II	1253.805	0.715	abs	−260
S II	1253.805	0.833	abs	−186
Si II(S II)	1260.42(,1259.5)	0.559	abs	−407
Si II	1260.422	0.715	abs	−344
Si II	1260.422	0.833	abs	−230
O I	1302.1685	0.559	abs	−328
O I	1302.1685	0.715	abs	−330
O I	1302.1685	0.833	abs	−216
Si II	1304.3702	0.559	abs	−307
Si II	1304.3702	0.715	abs	−308
Si II	1304.3702	0.833	abs	−230
C II	1334.532	0.559	abs	−383
C II	1334.532	0.715	abs	−320
C II	1334.532	0.833	abs	−210
O v	1371.292	0.559	1.62(−13)	−163
O v	1371.292	0.715	1.60(−13)	−228
O v	1371.292	0.833	2.35(−13)	−212
Si IV	1393.755	0.559	1.27(−13)	−293
Si IV	1393.755	0.596	9.7(−14)	−168
Si IV	1393.755	0.715	1.21(−13)	−210
Si IV	1393.755	0.723	1.15(−13)	−154
Si IV	1393.755	0.833	1.36(−13)	−134
Si IV	1393.755	0.841	1.36(−13)	−153
Si IV,O IV] blend	1402.77	0.559	3.7(−13)	−261
Si IV blend	1402.77	0.596	3.50(−13)	−174
Si IV blend	1402.77	0.715	3.00(−13)	−58
Si IV blend	1402.77	0.723	2.92(−13)	−37
Si IV blend	1402.77	0.833	2.50(−13)	+62
Si IV blend	1402.77	0.841	2.43(−13)	+80
N IV	1486.496	0.596	8.1(−14)	−216
N IV	1486.496	0.723	4.6(−14)	−189
N IV	1486.496	0.841	4.0(−14)	NA
C IV	1548,1550	0.596	7.78(−13)	NA
C IV	1548,1550	0.723	7.20(−13)	NA
C IV	1548,1550	0.841	6.23(−13)	NA
He II	1640.5	0.596	2.61(−13)	−202
He II	1640.5	0.723	2.45(−13)	−227
He II	1640.5	0.841	2.19(−13)	+45

[a] In ergs s^{-1} cm^{-2} $Å^{-1}$; "abs" indicates an absorption line.
[b] In km s^{-1} for peak of narrow lines, average for broad lines.

$v \approx 220$ km s^{-1}, the flux is greater in the red doublet component than in the blue component, that is, $F_{1238}/F_{1242} \approx 0.89$. This ratio reaches a minimum of $F_{1238}/F_{1242} \approx 0.75$ at a velocity of ≈ 325 km s^{-1}.

This puzzling doublet ratio is neither an instrumental artifact nor a statistical fluctuation. The 1238 Å line peaks at about 200 counts per diode, while the 1242 Å line peaks at about 300 counts per diode. (The ratio of fluxes F_{1238}/F_{1242} is not the same as the ratio of count rates because the sensitivity of the GHRS varies with wavelength.) Therefore, the noise in the 1242 Å line is $\approx 6\%$ of the flux, and the noise in the 1238 Å line is $\approx 7\%$. The flux ratio therefore has an uncertainty of $\approx 13\%$ so that a ratio of $F_{1238}/F_{1242} = 0.75$ in a single diode is not particularly significant ($\approx 2\ \sigma$). However, the reversed doublet ratio persists over 11 diodes. In this range (spanning velocities from +220 km s^{-1} to +360 km s^{-1}), $F_{1238}/F_{1242} = 0.87 \pm 0.035$. Uncertainty from sources other than counting statistics should be negligible. The variations of diode sensitivity should be of order $\lesssim 1\%$, and summing over 11 diodes greatly reduces this contribution to the error.

4. LOW-RESOLUTION OBSERVATIONS

The low-resolution observations (summarized in Table 3) show clearly that as the orbit advanced, all the emission lines became weaker and broader. All exposures were either in the wavelength range of 1200–1470 Å or in the range of 1380–1650 Å. In Figure 4, we show both the short-wavelength and long-wavelength observations, combined at nearby orbital phases to produce spectra in the range of 1200–1650 Å. The small differences between the two spectra in the wavelength range where they overlap can be attributed to a combination of time variability in the source and slight differences in spectrometer calibration. We estimate that the velocities inferred from the low-resolution observations may be in error by as much as 150 km s^{-1}.

The most prominent emission lines are due to N v (1240 Å), O v (1370 Å), Si IV (1393, 1403 Å), N IV (1486 Å), C IV

(1550 Å), and He II (1640 Å). All these lines have been detected with *IUE* (Howarth & Wilson 1983) and with the FOS (Anderson et al. 1994). We assume the absorption features are interstellar.

The Si IV line at 1403 Å is superimposed on a blended O IV] multiplet at 1401.2, 1404.8, and 1407.4 Å. While this feature can provide a density diagnostic, our resolution and sensitivity were not sufficient to apply this method. In addition, a S IV line at 1404.8 Å and a S VI line at 1406.1 Å may complicate analysis (Cook et al. 1995).

5. PULSATIONS IN THE UV CONTINUUM

We detected pulsations in the UV continuum of Her X-1 at $\phi_{\rm orb} = 0.56$ and $\phi_{\rm orb} = 0.83$. These pulsations were similar in amplitude ($\sim 0.5\%$) to the optical continuum pulsations previously reported (Davidsen et al. 1975; Groth 1974; Middleditch & Nelson 1976; Nelson, Chanan, & Middleditch 1977). The pulsations we observed with *HST* also occurred at orbital phases at which optical pulsations are typically seen. At $\phi_{\rm orb} \approx 0.75$, optical pulsations are prominent, with pulse Doppler shifts corresponding to both HZ Her and the neutron star (Middleditch & Nelson 1976).

We applied several methods to determine the significance of pulsations in the UV continuum. The most straightforward method is the power spectrum (Figs. 5*a* and 5*c*). We took power spectra of counts in the entire wavelength region available to us with the G140L grating (1200–1490 Å), but excluded the region surrounding the strong geocoronal Lyα line at 1216 Å. The results show prominent signals (9–15 times the average power) at redshifted velocities betwen 0 and 500 km s^{-1}.

We also applied the Analysis of Variance (ANOVA) technique to determine the pulse frequency (Davies 1990, 1991) and to provide another estimate of the statistical significance of the pulsations. Power spectra are limited to a frequency resolution of $1/T$, where T is the total observation time. For our observations, this limits us to a velocity resolution of ~ 150 km s^{-1}.

The ANOVA tests show that the centroids of the probability peaks occur near velocities expected for the neutron star's orbit. However, the ANOVA periodograms also show some structure at other velocities (Figs. 5*b* and 5*d*). It is not clear whether this structure represents sidebands of a signal at the neutron star's velocity, or whether there are several reprocessing regions. ANOVA periodograms of simulated data also show strong sidebands. At $\phi = 0.56$, the Doppler velocities of the neutron star and the L1 point are separated by only 40 km s^{-1}, so that it is difficult to determine the origin of the observed UV continuum pulsations. For example, there is a strongly pulsed component at ≈ 10 km s^{-1}, which is near the expected velocity at the L1 point (Fig. 5). We note that there is no evidence for blueshifted pulsations (similar to the anomalous pulsations reported by Middleditch 1983) at $\phi_{\rm orb} = 0.56$.

Observations with the *Einstein Observatory* (McCray et al. 1982) show that the soft ($E < 0.85$ keV) and hard X-rays are out of phase by 240°. We must therefore compare the UV pulse profiles separately with the soft and hard X-ray pulses.

We examine the pulse waveforms by folding the UV continuum light curves over the pulsar spin period. We compensate for the motion of the neutron star and for a 2 leap-second difference between *ASCA* time and UTC (Day et al. 1995). Then we find that the UV continuum pulsation at $\phi_{\rm orb} = 0.83$ resembles the high-energy X-ray pulsation observed during the *ASCA* orbit prior to the pre-eclipse dip (Fig. 6). To compare the pulsations in different wavebands, it is useful to find a time offset ("delay" or "lag") at which the rms difference between the pulse waveforms is minimized. The UV continuum pulsation at $\phi = 0.56$ (Fig. 7) is not clearly aligned with the X-ray pulsation in either energy band, although the delay is ≈ 0.25 s (UV leading the soft

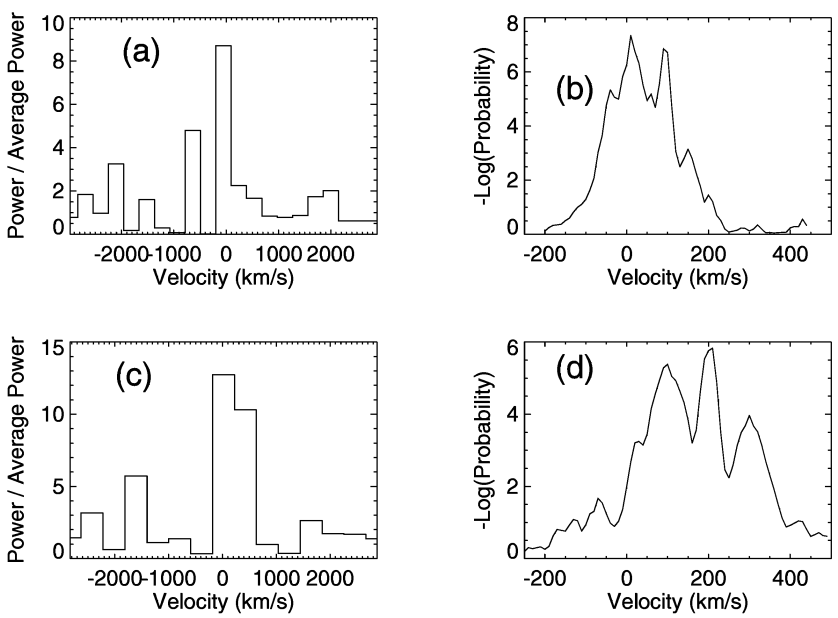

FIG. 5.—(*a*) Power spectrum of the UV continuum at $\phi_{\rm orb} = 0.56$. (*b*) ANOVA periodogram of the UV continuum at $\phi_{\rm rmorb} = 0.56$. We plot the nondetection probability against the velocity shift from the Her X-1 pulse period. (*c*) Power spectrum of the UV continuum at $\phi_{\rm orb} = 0.83$. (*d*) ANOVA periodogram of the UV continuum at $\phi_{\rm orb} = 0.83$.

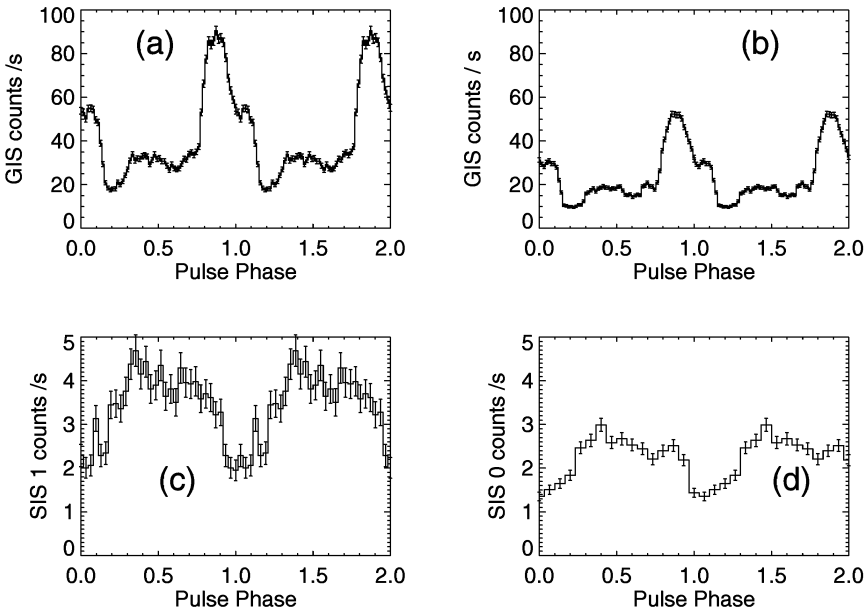

FIG. 6.—X-ray pulse profiles as determined by *ASCA*. (*a*) Hard X-ray pulse profile (0.8–10 keV) near $\phi_{orb} = 0.56$, observed with both the GIS 2 and the GIS 3. (*b*) Hard X-ray pulse profile (0.8–10 keV) near $\phi_{orb} = 0.75$, observed with the GIS. (*c*) Soft X-ray pulse profile (0.2–0.82 keV) near $\phi_{orb} = 0.56$, observed with the SIS 1. (*d*) Soft X-ray pulse profile at $\phi_{orb} = 0.75$, observed with the SIS 0.

X-rays) and there is an intrinsic 0.125 s uncertainty in the start time of the GHRS observations.

The rms pulsed fraction of the UV continuum was 4×10^{-3} at $\phi_{orb} = 0.56$ and 7×10^{-3} at $\phi_{orb} = 0.83$. (The pulsed fluxes are similar because the UV continuum is brighter at $\phi_{orb} = 0.56$.) These pulse fractions are somewhat larger than the pulse fractions of the optical pulsations (typically 2×10^{-3}; Middleditch & Nelson 1976).

The power spectra also display $1/f$ noise. At $\phi_{orb} = 0.56$, the $1/f$ noise causes a 5.3% rms variation in the UV continuum, while at $\phi_{orb} = 0.83$, the $1/f$ noise causes a 3.8% rms variation. At orbital phases when no UV continuum pulse is seen, we still see $1/f$ noise with $\approx 3.5\%$ rms variation.

6. PULSATIONS IN THE N v LINES

We also found evidence for pulsations in the N v line at $\phi_{orb} = 0.80$. These pulsations only occurred in a narrow region (0.25 Å) near the peak of the weaker doublet component (at 1242.8 Å).

The power spectrum (Fig. 8) shows a peak of 9.6 times the average power at a frequency shifted by ≈ 300 km s^{-1} from the fundamental (at period 1.2377465 s). The probability of such a peak arising from noise is $\approx 7 \times 10^{-5}$. Application of ANOVA tests for periodicity give a similar probability (Fig. 9) and show that the pulsation is strongest at a frequency corresponding to $+235$ km s^{-1}. The redshift of the frequency matches well with the region of the N v line in which the pulsation occurs (Fig. 10), which has a Doppler shift of $+228$ km s^{-1}. (The pulse Doppler shift and wavelength Doppler shift can disagree for certain geometrical arrangements of the X-ray pulsar and the UV-emitting material.) Given that we searched a range of wavelengths, several time-resolved exposures, and several possible Doppler-shifted frequencies, we estimate that the nonde-

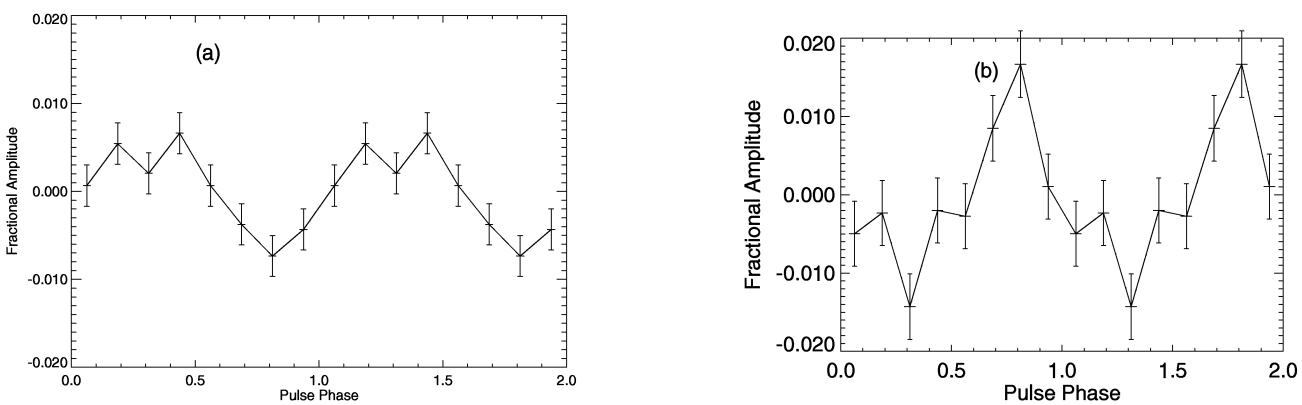

FIG. 7.—Profiles of the UV continuum pulsation at (*a*) $\phi_{orb} = 0.56$ and (*b*) $\phi_{orb} = 0.83$. We use the same pulse ephemeris for all continuum, N v line, and X-ray pulse profiles. The motion of the neutron star has been accounted for in the pulse arrival times.

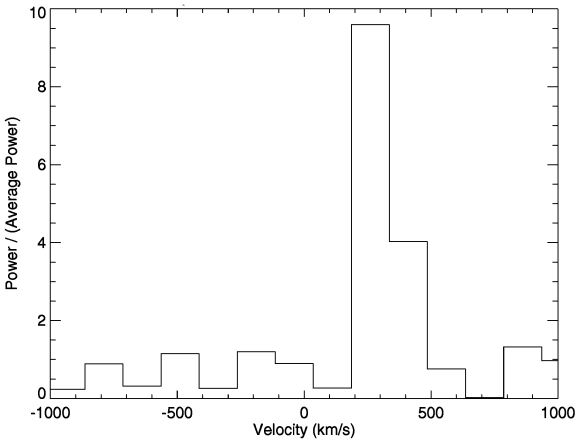

FIG. 8.—Power spectrum of a less than 1 Å region of the N v emission at $\phi_{orb} = 0.80$.

tection probability should be multiplied by ≈ 100 independent trials. The detection of N v line pulsations is not as secure as our detection pulsations in the UV continuum, as a result of the freedom of choosing a wavelength region within the N v doublet.

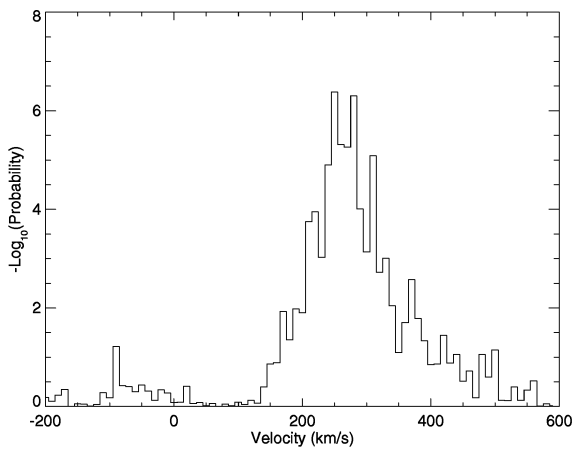

FIG. 9.—Application of an ANOVA test of periodicity in the N v line at 1242 Å.

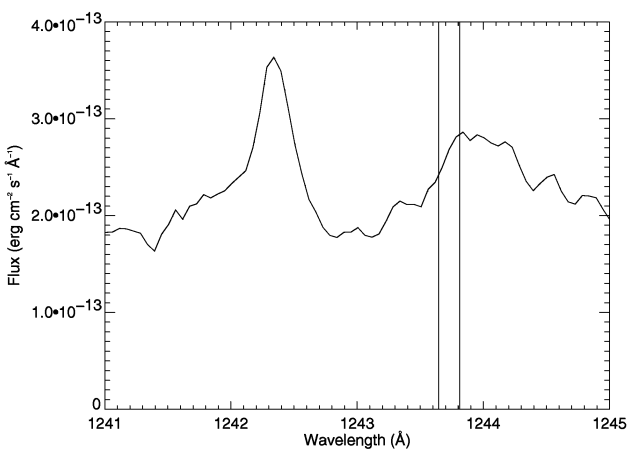

FIG. 10.—Region of the N v line in which we found pulsations. The continuous curve shows the spectrum at $\phi_{orb} = 0.80$ (smoothed with a 3 pixel boxcar average). The vertical lines indicate the pulsed region.

We are unable to determine a "delay" between the X-ray pulsations and the N v pulsations because the pulse frequencies differ. From the power spectral peak, we estimate a pulsed fraction of $\approx 15\%$ within the pulsed N v line region.

7. DISCUSSION

Joss et al. (1980) have reported the only previous comparison of simultaneous X-ray and optical continuum pulsations from Her X-1. They found that the delay between the hard X-ray and optical pulsations was 0.03 ± 0.06 s (X-rays lagging the optical pulsations, but consistent with no delay) at $\phi_{orb} \approx 0.8$. The pulse frequency of the optical pulsations matched the Doppler shift of the neutron star.

We found a similar result in our observation of continuum pulsations at $\phi_{orb} = 0.83$. The UV continuum pulsation led the hard X-ray pulsation by 0.1 ± 0.08 s (consistent with no delay). This suggests that the reprocessing region may be along the line of sight, where light travel times do not smear a reprocessed pulse.

The X-ray dips are also caused by material along the line of sight and are seen at orbital phases near the periods when we saw UV continuum pulsations, so it seems reasonable to identify the continuum pulsations with the same material that causes the dips. The anomalous dips result from absorbing column densities that are a factor of ≈ 3 lower than those observed during the pre-eclipse dips. Thus, the UV pulses observed near the anomalous dip should be caused by material that is illuminated by both hard and soft X-rays. This may lead to a UV continuum pulse profile with phase origin between that of the soft and hard X-rays.

The greater absorption of X-rays during the pre-eclipse dip can explain the correlation between the hard X-ray and the UV pulses, but one might then expect to see *weaker* UV continuum pulsations near the pre-eclipse dip. We can explain the strength of the UV pulsation during the pre-eclipse dip if the dip material not only attenuates the X-rays seen by the reprocessing material but is also the source of the UV pulses. The UV pulses at $\phi_{orb} = 0.83$ may be as strong as those at $\phi_{orb} = 0.56$ because there is more material along the line of sight to reprocess the X-rays.

However, this interpretation requires that the UV continuum pulsation at $\phi_{orb} = 0.56$ arise from material moving near the velocity of the neutron star, and we are unable to distinguish between pulse shifts due to the motion of the neutron star and the L1 point at this orbital phase. In an alternate scenario, the atmosphere of HZ Her could cause the UV continuum pulsations. The connection between the dip at $\phi_{orb} = 0.53$ and the UV pulsations at $\phi_{orb} = 0.56$ may be spurious; we may have detected pulsations at this phase only because our search was most sensitive when we used the 0.1 s readout. The time for X-rays to travel from the neutron star to the L1 point and for the resulting UV continuum photons to travel back toward the viewer should be greater than the pulse period of Her X-1. As a result, we have no clear expectation of the UV continuum pulse phase if the X-ray pulses are reprocessed by HZ Her. Further observations may be needed to determine the origin of the $\phi = 0.56$ pulsations.

We interpret the dramatic change in the C IV doublet (seen in our low-resolution spectra, § 4) in light of the medium-resolution observations of N v (§ 3). As the orbit progresses, the narrow N v components become weaker and vanish some time after $\phi_{orb} = 0.80$. The C IV doublet components are separated by only 2.6 Å, which corresponds

to 500 km s^{-1}. If the C IV lines are similar to the N V lines, then after $\phi_{orb} = 0.80$, the narrow component of the C IV lines should disappear, leaving only a component nearly as broad as the doublet separation. The resolution of the G140L grating ($\approx$150 km s^{-1}) should further broaden the profile, thus explaining the merger of the C IV doublet components in our spectra at late orbital phases.

As the orbit progressed, the Si IV and O V emission lines became double-peaked. This is a typical signature of emission from the surface of an accretion disk (Smak 1969; Huang 1972). The velocity separation between the peaks (570 ± 70 km s^{-1}, averaged over the double-peaked lines at $\phi = 0.83, 0.84$), would be typical for an accretion disk with radius $\sim 2 \times 10^{11}$ cm. We do not see a double-peaked shape in the medium-resolution N V exposures (§ 3), although the FWHM of the broad N V lines (850 km s^{-1}) is similar to that of the double-peaked lines (1000–1450 km s^{-1}) observed at low-resolution.

If the narrow lines originate on the X-ray–heated face of HZ Her, we would expect that they would be brightest near $\phi_{orb} = 0.5$, when the tip of HZ Her near the L1 point (closest to the X-ray source) is facing the line of sight. This is consistent with our observations.

Although we identify the narrow lines with the X-ray–heated face of HZ Her, they are broader than we expect from the Doppler velocities caused by the synchronous rotation of the star with the binary orbit (Fig. 11). As we shall discuss in Paper III, we believe that the line widths indicate X-ray–driven mass loss from the atmosphere of HZ Her.

The broad lines at $\phi_{orb} = 0.88$ and $\phi_{orb} = 0.91$ are apparently uncontaminated by narrow-line emission. Thus, these lines should be a clear indication of the structure of the accretion disk. The breadth of the lines (FWHM $\approx$ 800–900 km s^{-1}) corresponds to velocities typical of the edge of an accretion disk of radius $\sim 2 \times 10^{11}$ cm.

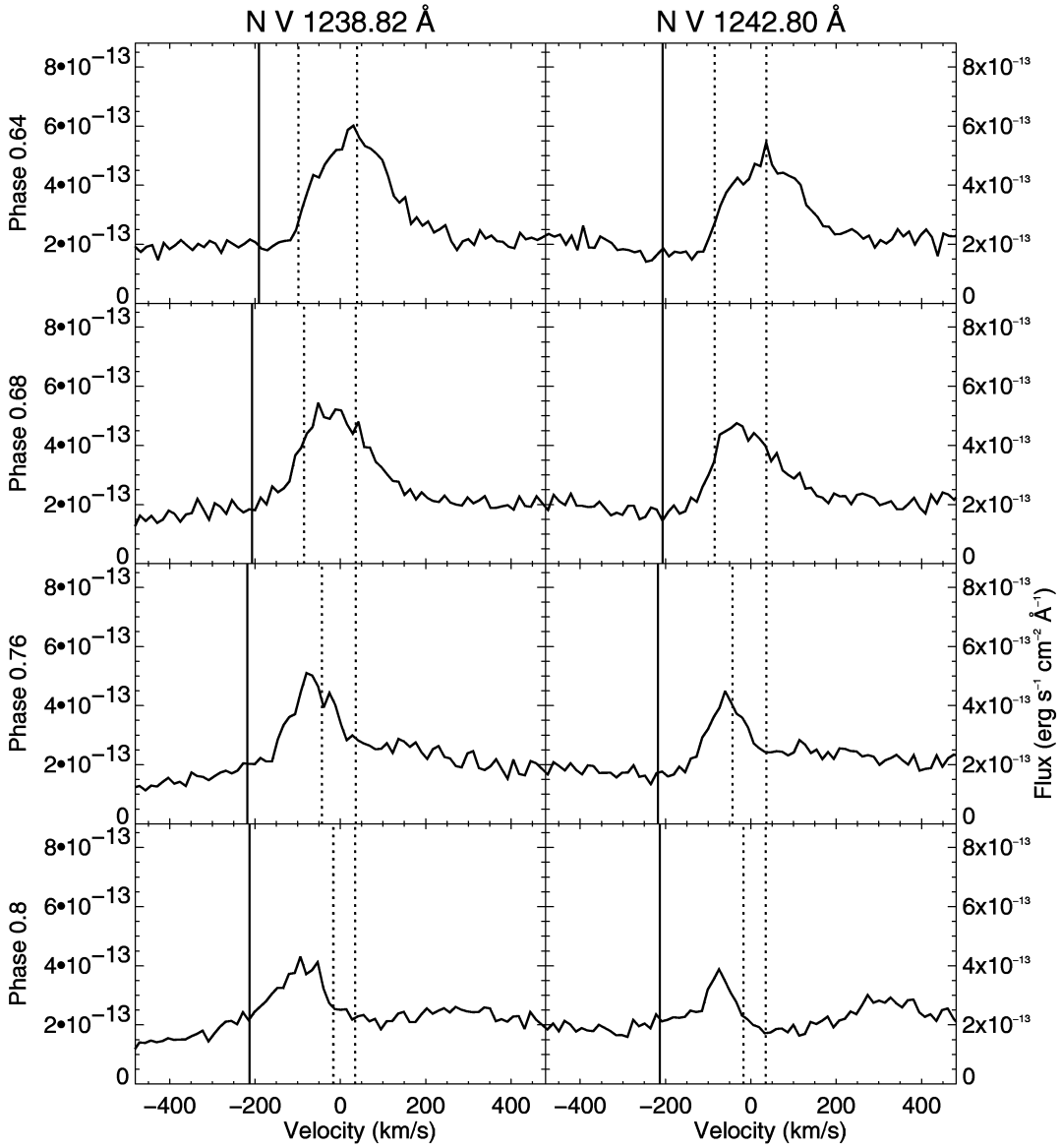

FIG. 11.—Orbital variation of the narrow N V lines, which we attribute to the X-ray–heated face of HZ Her. The graphs in the left column show the N V line at 1238.8 Å, while the graphs in the right column show the N V line at 1242.8 Å. Orbital phases $\phi_{orb} = 0.64$ through $\phi_{orb} = 0.80$ are shown in each row. Vertical dashed lines show the velocity range arising from the rotation of the unocculted X-ray–heated face of HZ Her. The vertical solid line shows the velocity limit if we include those regions of HZ Her which are not illuminated by direct X-rays.

The shape of the N v lines may indicate the shape and ionization of the accretion disk. While the doublet ratio indicates that the optical depth is greater in the broad lines than in the narrow lines, the blue line is stronger at $\phi_{orb} = 0.88$ by $\approx 20\%$. We expect lines formed in the accretion disk to be optically thick (Raymond 1994) as the lines seen at $\phi_{orb} = 0.91$ appear to be. There may be other sources of emission and absorption in the system (such as the gas stream between the two stars) that complicate the analysis.

Between $\phi_{orb} = 0.88$ and $\phi_{orb} = 0.91$, the flux near the blue edge of the broad N v lines decreased dramatically. This probably results from the eclipse of the accretion disk by the surface of HZ Her. This interpretation implies that the accretion disk rotates in a prograde direction with respect to the orbit. In Paper III we will explore the implications of our eclipse-ingress data for both the structure of the accretion disk and for the size of the atmosphere of HZ Her.

The doublet ratio of the broad N v lines at $\phi_{orb} = 0.80$ suggests that the lines do not originate in a uniform emitting and self-absorbing slab. The oscillator strength of the N v transition at 1242.804 Å is half that of the 1238.821 transition, so such a uniform slab should give rise to intensities $I_{1242} = S[1 - \exp(-\tau)]$ and $I_{1238} = S[1 - \exp(-2\tau)]$. Here τ and S are the optical depth in the weaker line and the source function, respectively. For small τ, we have $F_{1242} \approx S\tau$ and $F_{1238} \approx 2S\tau = 2F_{1242}$. The ratio $R = F_{1238}/F_{1242} = [1 - \exp(-2\tau)]/[1 - \exp(-\tau)]$ decreases monotonically from $R = 2$ for $\tau \to 0$ to $R = 1$ for $\tau \to \infty$.

The 3–4 σ reversal of the doublet ratio is significant in the context of the rest of the spectrum. The peaks of the two doublet components differ in velocity (≈ 250 km s^{-1} for the red line and ≈ 300 km s^{-1} for the blue line). In addition, the broad line emission is stronger at this orbital phase than at any other we observed. In Paper III, we explain the doublet ratio as the result of overlapping P Cygni profiles, in which the blueshifted absorption of the 1242 Å component diminishes the flux in the 1238 Å emission. P Cygni scattering would also explain the enhanced flux throughout the broad N v lines compared with other orbital phases.

The broad N v lines at $\phi_{orb} = 0.80$ have a Doppler shift corresponding to the motion of the neutron star, so the P Cygni lines are probably associated with an outflow from the disk or a portion of the disk. P Cygni lines corresponding to expansion velocities of ~ 3000 km s^{-1} are seen in cataclysmic variables (Drew 1993). For Her X-1, P Cygni lines have been reported once before (Koo & Kron 1977), for just one spectrum of Hβ (at $\phi_{orb} = 0.97$) among a series of many optical spectra. A disk wind would also be consistent with the persistence of UV lines during eclipse (Anderson et al. 1994) and the residual X-ray flux during eclipse and the off-state (Choi et al. 1994). Our observation requires that the outflow velocity of the wind be ≈ 1000 km s^{-1} in order for the lines to overlap without producing absorption troughs, which are not observed.

The reversed doublet ratio was only observed during this one exposure at $\phi_{orb} = 0.80$, which coincided with a pre-eclipse X-ray dip. Thus there is likely to be a connection between the dips and the P Cygni lines, as there may be a connection between the dips and the UV continuum pulsations.

8. FUTURE WORK

We have presented the results and some preliminary explanations of our successful GHRS observation of Her X-1. In Papers II and III, we will use these observations to investigate the size and velocity field of the Roche lobe of HZ Her, the twisted nature of the disk, the presence of a disk wind, and the cause of the reprocessed pulsations.

This work is based on observations with the NASA/ESA *Hubble Space Telescope*, obtained at the Space Telescope Science Institute, which is operated by the Association of Universities for Research in Astronomy, Inc., under NASA contract NAS 5-26555. We would like to acknowledge a NASA Long-Term Space Astrophysics grant (NAGW-2685).

We are grateful to Tony Roman, Peg Stanley, and the Observation Support team at STScI for their assistance in planning the *HST* observation. Stephen Hulbert, Lisa Sherbert, and Ron Gilliland helped us understand the GHRS and its RAPID mode. Koji Mukai and Christopher Becker helped us to plan the *ASCA* observation, and Keith Arnaud helped us to reduce the *ASCA* data. Masaharu Hirayama helped us convert from spacecraft time to barycentric time.

REFERENCES

Anderson, S. F., Wachter, S., Margon, B., & Downes, R. A. 1994, ApJ, 436, 319
Bahcall, J. N., & Bahcall, N. A. 1972, ApJ, 1978, L1
Boyle, S., Howarth, I., Wilson, R., & Raymond, J. 1986, in ESA Proc. Int. Symp. on New Insights in Astrophysics, ed. E. J. Rolfe (Noordwijk; The Netherlands: ESA), 471
Cheng, F. H., Vrtilek, S. D., & Raymond, J. C. 1995, ApJ, 452, 825
Choi, C. S., Dotani, T., Nagase, F., Makino, F., Deeter, J. E., & Min, K. W. 1994, ApJ, 427, 400
Cook, J. W., Kennan, F. P., Dufton, P. L., Kingston, A. E., Pradhan, A. K., Zhang, H. L., Doyle, J. G., & Hayes, M. A. 1995, ApJ, 444, 936
Crampton, D., & Hutchings, J. B. 1974, ApJ, 191, 483
Crosa, L., & Boynton, P. E. 1980, ApJ, 235, 999
Davidsen, A., Margon, B., & Middleditch, J. 1975, ApJ 198, 653
Davies, S. R. 1990, MNRAS, 244, 93
———. 1991, MNRAS, 251, 64P
Day, C., Arnaud, K., Ebisawa, K., Gotthelf, E., Ingham, J., Mukai, K., & White, N. 1995, The ABC Guide to *ASCA* Data Reduction
Drew, J. E. 1993, Cataclysmic Variables and Related Physics: Second Technion Haifa Conference, ed. O. Regev & G. Shaviv (New York: AIP), 128
Dupree, A. K., et al. 1978, Nature, 275, 400
Giacconi, R., Gursky, H., Kellogg, E., Levinson, R., Schreier, E., & Tananbaum, H. 1973, ApJ, 184, 227
Groth, E. J. 1974, ApJ, 192, 517
Howarth, I. D., & Wilson, R. 1983, MNRAS, 204, 1091
Huang, S. 1972, ApJ, 1971, 549
Joss, P. C., Li, F., Nelson, J., & Middleditch, J. 1980, ApJ, 235, 592
Koo, D. C., & Kron, R. G. 1977, PASP, 89, 285
McCray, R., Shull, J. M., Boynton, P. E., Deeter, J. E., Holt, S. S., & White, N. E. 1982, ApJ, 262, 301
Margon, B., Davidsen, A., & Bowyer, S. 1976, ApJ, 208, L35
Middleditch, J. 1983, ApJ, 275, 278
Middleditch, J., & Nelson, J. 1976, ApJ, 208, 567
Milgrom, M., & Salpeter, E. E. 1975, ApJ, 196, 589
Ögelman, H. 1987, A&A, 172, 79
Nelson, J., Chanan, G. A., & Middleditch, J. 1977, ApJ, 212, 215
Petterson, J. A. 1975, ApJ, 201, L39
Raymond, J. 1994, ApJ, 412, 267
Smak, J. 1969, Acta Astron., 19, 155
Soderblom, D. R., & the STScI GHRS Team. 1993, Goddard High Resolution Spectrograph Instrument Handbook
Tananbaum, H., Gursky, H., Kellog, E. M., Levinson, R., Schrier, E., & Giacconi, R. 1972, ApJ, 174, L143
Vrtilek, S. D., & Cheng, F. H. 1996, ApJ, 465, 915